Manifestation of Topological Protection in Transport Properties of Epitaxial Bi_2Se_3 Thin Films

A. A. Taskin, Satoshi Sasaki, Kouji Segawa, and Yoichi Ando*

Institute of Scientific and Industrial Research, Osaka University, Ibaraki, Osaka 567-0047, Japan

(Received 9 April 2012; published 9 August 2012)

The massless Dirac fermions residing on the surface of three-dimensional topological insulators are protected from backscattering and cannot be localized by disorder, but such protection can be lifted in ultrathin films when the three-dimensionality is lost. By measuring the Shubnikov–de Haas oscillations in a series of high-quality Bi_2Se_3 thin films, we revealed a systematic evolution of the surface conductance as a function of thickness and found a striking manifestation of the topological protection: The metallic surface transport abruptly diminishes below the critical thickness of ~6 nm, at which an energy gap opens in the surface state and the Dirac fermions become massive. At the same time, the weak antilocalization behavior is found to weaken in the gapped phase due to the loss of π Berry phase.

DOI: 10.1103/PhysRevLett.109.066803 PACS numbers: 73.25.+i, 71.18.+y, 72.20.My, 73.20.At

In topological insulators (TIs) the energy states are fundamentally modified from ordinary insulators by strong spin-orbit interactions, giving rise to a topologically distinct state of matter with a gapped insulating bulk and a gapless metallic surface [1]. Various interesting phenomena, including surface transport of spin-filtered Dirac fermions that are immune to localization, have been predicted and raised expectations for novel applications [2–4]. However, the progress in real applications of TIs crucially relies on the ability to manipulate the surface current in transport experiments. At present, such basic characterization as the surface conductance measurement has been possible only in a few cases in single crystals [5–12] because of the dominance of bulk transport caused by unintentional doping due to defects. Molecular beam epitaxy (MBE) is a promising technique for the synthesis of TIs [13–18] owing, in part, to the relatively low deposition temperature at which defect concentrations can be reduced from those in bulk crystals grown in thermal equilibrium. So far, using MBE-grown films, angle-resolved photoemission spectroscopy (ARPES) [19] and scanning tunneling spectroscopy (STS) [20] have provided useful information about the topological surface state (SS), and in transport experiments, such phenomena as weak antilocalization (WAL) and gate-controlled ambipolar transport have been reported [21,22]. Also, since the MBE technique gives a precise control over film thickness, transport measurements for widely varying surface-to-bulk conductivity ratio have been performed [23–25], although a reliable separation of surface Dirac electrons from bulk carriers has been hindered by a relatively low mobility of carriers in available thin films. Recently, we have succeeded in growing high-quality epitaxial films of Bi_2Se_3 that have a sufficiently high surface electron mobility to present pronounced Shubnikov–de Haas (SdH) oscillations. This made it possible to directly probe the surface conductance and the topological protection of the SS.

The immunity of the surface Dirac fermions to localization has a twofold origin [1–3]. One is the π Berry phase associated with massless Dirac fermions [26], which protects them from weak localization through destructive interference of time-reversed paths. The other is the peculiar spin-momentum locking which nulls the backscattering probability [1–3]. Those mechanisms are collectively called topological protection. Recently, it was found [19,27–31] that when TIs are thinned to the extent that the top and bottom surface states feel each other, their hybridization leads to an opening of the gap at the Dirac point and results in a degenerate, massive Dirac dispersion. This gapped state obviously violates the topological protection, but its consequence in the surface transport properties has not been duly addressed. In fact, this question is important because recently a lot of attention has been paid to the way to open a gap at the Dirac point [32] to realize topological magnetoelectric effects [33]. One may expect that unless the chemical potential is located exactly within the gap, the metallic surface transport is largely unaffected by the gap opening because states are kept being available for transport at the Fermi level. However, in the present work it turned out that the change in the Dirac spectrum deep in the occupied state has a profound effect on the physics at the Fermi level.

The growth of Bi_2Se_3 films occurs in a layer-by-layer manner, in which the 0.95-nm thick Se-Bi-Se-Bi-Se quintuple layer (QL) constitutes the basic unit [19]. Our systematic magnetotransport measurements for varying thickness reveal a sudden diminishment of the surface transport below the critical thickness of ~6 QL, below which the energy gap opens in the Dirac spectrum [19]. We also observed that the weak antilocalization behavior [21,22] quickly weakens below the critical thickness. We discuss that those striking effects are due to acquired degeneracy of the surface states [29] and loss of their π Berry phase [34,35] in the gapped phase.

 © 2012 American Physical Society

Our MBE films were grown under Se-rich conditions on insulating sapphire (0001) substrates whose size was approximately 15×4 mm^2. To obtain films of high enough quality to present SdH oscillations, we employed a two-step deposition procedure [36,37]. Both Bi (99.9999%) and Se (99.999%) were evaporated from standard Knudsen cells. The $Se_2(Se_4)/Bi$ flux ratio was kept between 15–20. The growth rate, which is determined by the Bi flux, was kept at 0.2–0.3 QL/min. The resistance R_{xx} and the Hall resistance R_{yx} were measured in the Hall bar geometry by a standard six-probe method on rectangular samples on which the contacts were made with silver paste at the perimeter and cured at room temperature under pressure of $\sim$1 Pa. The magnetic field was swept between $\pm$14 T at fixed temperatures and was always applied perpendicular to the films, except for the angular-dependence measurements of the Shubnikov–de Haas oscillations.

An atomic force microscopy (AFM) image of our relatively thick (50 QL) film is shown in Fig. 1(a), where a large, atomically flat area of $\sim$1 μm^2 and several sharp terraces with the height of exactly 1 QL can be clearly seen. The reflection high-energy electron diffraction (RHEED) pattern with sharp 1×1 streaks [Fig. 1(a) inset] and sharp x-ray diffraction peaks [Fig. 1(b)] are also indications of the high crystal quality of our films.

Temperature dependencies of the sheet resistance, $R_S(T)$, measured in films with systematically changed thickness t down to 2 QL are shown in Fig. 1(c). The $R_S(T)$ behavior is metallic in thick films, but below $t = 5$ QL, it starts to show an upturn at low temperatures. In particular, the sharp divergence in R_S for $T \to 0$ in the 2-QL film is indicative of strong Anderson localization and an insulating ground state (see Supplemental Material [37]).

The breakthrough in the present work is that our films exhibit pronounced two-dimensional (2D) SdH oscillations

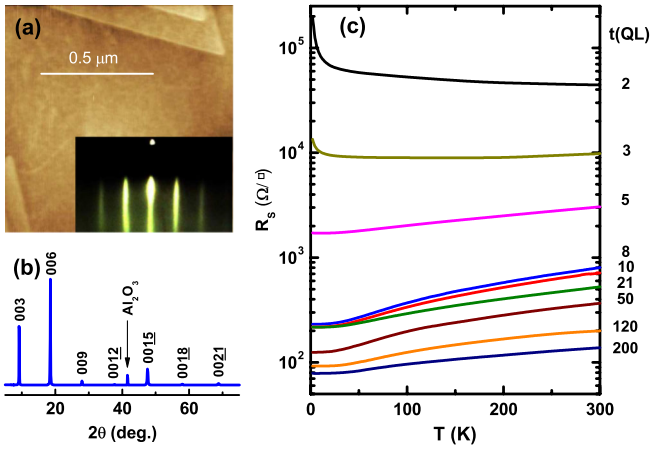

FIG. 1 (color online). (a) AFM image of a 50-nm thick Bi_2Se_3 film showing atomically flat terraces with 1-QL steps. Inset: typical RHEED pattern. (b) X-ray diffraction pattern of a 200-QL film. (c) Temperature dependences of R_s for different thickness.

to provide a direct way to probe the surface charge transport. As an example, the analysis of the SdH oscillations in the 10-QL film is shown in Fig. 2. The 2D character of the oscillations is evident in Fig. 2(a), where the positions of the maxima and minima depend only on the perpendicular component of the magnetic field, $B_\perp$. The oscillation frequency $F = 106.8$ T is obtained from the Fourier transform [lower inset of Fig. 2(c)], and this is a direct measure of the Fermi wave number $k_F = 5.7 \times 10^6$ cm^{-1}. As we discuss in detail in the Supplemental Material [37], if the SdH oscillations are due to the trivial 2D electron gas which may form due to a band bending near the surface [38], this k_F is so small that it imposes too strong a constraint on the possible bulk Fermi level, which makes it impossible to consistently explain the transport data. Hence, we identify the oscillations to be due to surface Dirac fermions, and the obtained k_F gives their density $n_s = 2.6 \times 10^{12}$ cm^{-2}.

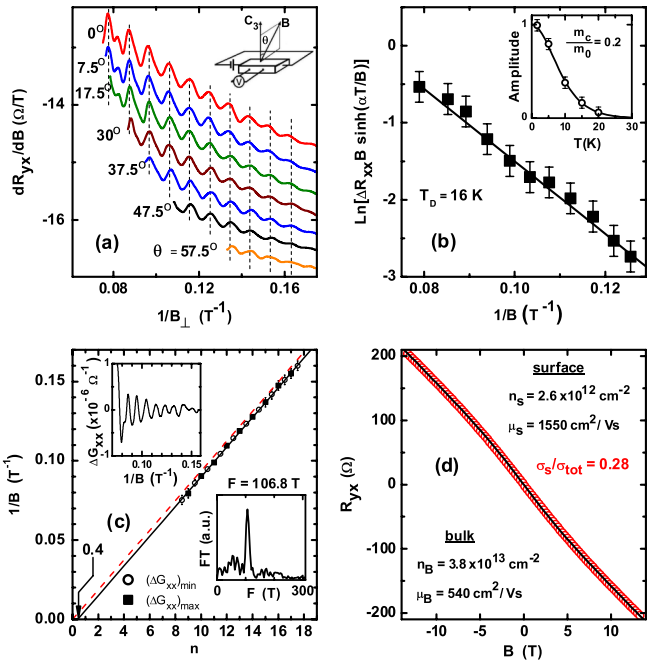

FIG. 2 (color online). Surface SdH oscillations in the 10-QL film. (a) dR_{yx}/dB in tilted magnetic fields, plotted as a function of $1/B_\perp$ ($= 1/B\cos\theta$); curves are shifted vertically for clarity. Dashed lines mark the positions of maxima. Inset shows the geometry of the experiment. (b) Dingle plot of the oscillations in ΔR_{xx} at 1.6 K, obtained after subtracting a smooth background from $R_{xx}(B)$, giving the Dingle temperature of 16 K. Inset: T-dependence of the SdH amplitude for $\theta = 0°$. (c) Landau-level fan diagram for oscillations in G_{xx} measured at $T = 1.6$ K and $\theta = 0°$; following Ref. [43], integers n (half-integers $n + \frac{1}{2}$) are assigned to the minima (maxima) in ΔG_{xx}. The solid line is a linear fitting to the data with the slope fixed at $F = 106.8$ T; the dashed line has the same slope and extrapolates to zero. Upper inset shows ΔG_{xx} vs $1/B$ after subtracting a smooth background; lower inset shows its Fourier transform giving $F = 106.8$ T. (d) Fitting of the two-band model to the $R_{yx}(B)$ data at 1.6 K.

In this 10-QL film, we observed only a single frequency, but we usually see two frequencies in other films (see Fig. S3 of the Supplemental Material [37]), suggesting that the top and bottom surfaces have somewhat different n_s. The temperature dependence of the oscillation amplitude [Fig. 2(b) inset] gives the cyclotron mass $m_c = 0.2m_0$ (m_0 is the free electron mass) [39] which in turn gives the Fermi velocity $v_F = 3.3 \times 10^7$ cm s^{-1}. This v_F is consistent with the ARPES data [40] as well as the STS data [20,41] for the Dirac cone. The obtained k_F value corresponds to the Fermi level of ~0.16 eV above the Dirac point for the topological surface state, which points to a slight upward band bending [42]. The Dingle analysis [Fig. 2(b); see the Supplemental Material [37] for details] yields the mobility $\mu_s = 1330$ cm^2 V^{-1} s^{-1}. Finally, Fig. 2(c) shows the Landau-level fan diagram for the oscillations in conductance G_{xx}, where the positions of the minima in ΔG_{xx} (shown in the upper inset) are plotted as a function of n [43]. Here, to minimize the error occurring from extrapolation [12], we fix the slope of the linear fitting by using $F = 106.8$ T obtained from the Fourier analysis and determine the intercept $n = 0.40 \pm 0.04$ (solid line); this is very close to the ideal value of 0.5 for Dirac electrons bearing the π Berry phase [44], giving further confidence in the origin of the SdH oscillations. For comparison, a straight line with the same slope to give zero Berry phase is shown in Fig. 2(c) with a dashed line, which is obviously inconsistent with the experimental data.

To estimate the contribution of the SS in the overall transport in this 10-QL film, we use the magnetic-field dependence of the Hall resistivity, $R_{yx}(B)$ [Fig. 2(d)], which is not linear in B and thus signifies the presence of at least two types of carriers. The fitting of a standard two-band model [6,8,45] to the data, in which n_s is fixed by the SdH frequency, gives the surface contribution to the total conductance, G_s/G_{tot}, of 28%. The μ_s value obtained from this fitting is close to the SdH result, assuring the consistency of our analysis.

The same analysis can be applied to all measured films with $t \geq 8$ QL, in which we consistently observed SdH oscillations [37]. Evolutions of the transport parameters with changing t are summarized in Figs. 3(a)–3(c). We note that by tracing the evolution of the SdH oscillations starting from thick films, we can distinguish the topological SS from the 2D quantum-well state of the bulk origin [37] as the source of the SdH oscillations.

Our main finding is that the surface transport abruptly diminishes below a critical thickness t_c which is located between 5 and 8 QL. This change is most convincingly manifested in the behavior of $R_{yx}(B)$, which suddenly becomes B-linear in films with $t \leq 5$ QL [Fig. 3(d)]; this indicates that the transport becomes suddenly dominated by only one type of carriers. Correspondingly, the SdH oscillations disappear for $t < t_c$. More quantitatively, assuming that n_s is essentially unchanged through t_c [dashed squares in Fig. 3(a)], one can estimate that μ_s must be suddenly degraded by more than an order of magnitude in samples with $t < t_c$ [dashed squares in Fig. 3(b)] for $R_{yx}(B)$ to become linear and be governed by bulk carriers [37]. The magnetoresistance behavior shown in Fig. 3(e) also presents a qualitative change below t_c, showing a negative slope at high fields. This evolution is best represented in the t dependence of G_s/G_{tot} [Fig. 3(c)], which shows a steady increase with decreasing t to reflect the change in the surface-to-bulk ratio, but it drops sharply below t_c to signify that the surface transport is abruptly diminished.

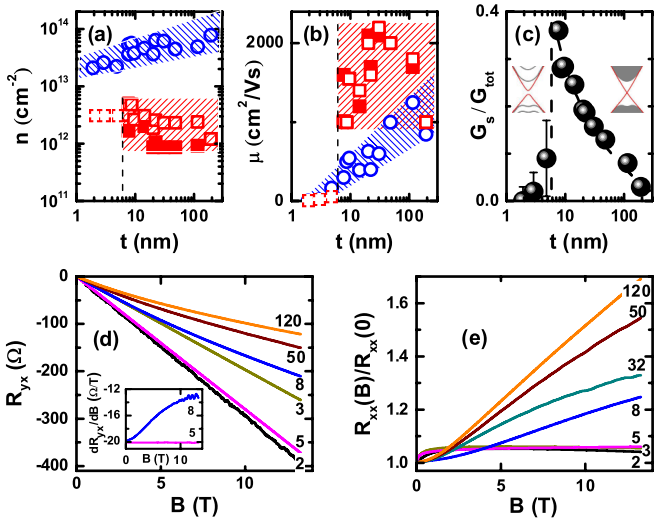

FIG. 3 (color online). (a) Squares are the n_s obtained from SdH oscillations (open and filled squares represent two different surfaces of the same film) and the dashed squares are an extrapolation of the trend above t_c; circles are the sheet density of bulk carriers obtained from two-band analyses. (b) Mobilities of surface (squares) and bulk (circles) carriers obtained from two-band analyses. (c) G_s/G_{tot} obtained from the data in (a) and (b). Insets are schematic pictures of the energy bands for the two regimes. (d) $R_{yx}(B)$ at 1.6 K for various thickness shown in QL unit; inset shows the derivative dR_{yx}/dB for the 5 and 8 QL films (5-QL data are shifted for clarity). (e) $R_{xx}(B)/R_{xx}(0)$ of the same films.

This observation naturally calls for the question whether the observed diminishment of the surface transport in ultrathin films might be related to a lowering of the quality in thinner films. In this respect, our ultrathin films remain essentially flat and smooth across t_c, with the surface bumpiness of only ~1 QL (see Fig. S10 in the Supplemental Material [37]). This observation, combined with the fact that G_s/G_{tot} increases steadily with decreasing t until it reaches t_c, testifies against the above concern.

In addition to the above results, we found a striking change in the WAL behavior [21,22] below $t = 5$ QL. Figure 4(a) shows the magnetoconductance of our films measured in perpendicular magnetic fields at 1.6 K. Dashed lines are the fitting with the Hikami-Larkin-Nagaoka formula [46],

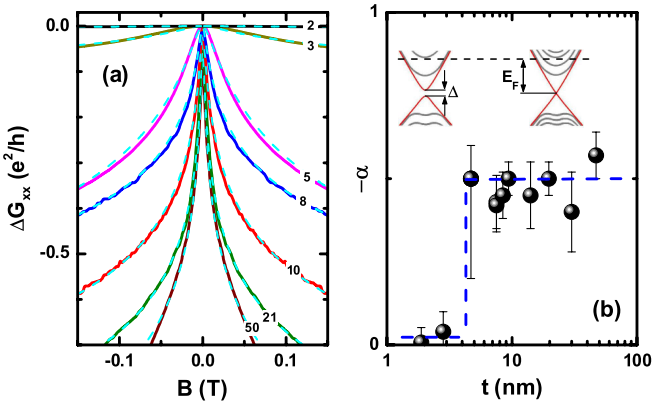

FIG. 4 (color online). (a) WAL behavior in sheet conductance at 1.6 K for various thicknesses shown in QL units; dashed lines are the fittings using Eq. (1). (b) Thickness dependence of α. Inset shows schematic energy bands above and below the critical thickness.

$$\Delta G_{xx}(B) = \alpha \frac{e^2}{\pi h}\left[\Psi\left(\frac{\hbar}{4eL_\phi^2 B}+\frac{1}{2}\right) - \ln\left(\frac{\hbar}{4eL_\phi^2 B}\right)\right], \quad (1)$$

where Ψ is the digamma function and L_ϕ is the phase coherence length. The prefactor α should be $-\frac{1}{2}$ for each transport channel that either carries a π Berry phase [26] or bears a strong spin-orbit interaction [46]. In our analysis, α and L_ϕ are the only fitting parameters and Fig. 4(b) shows the t dependence of obtained α (see the Supplemental Material [37] for details). For $t \geq 5$ QL, we observed $\alpha \approx -\frac{1}{2}$ similar to that reported for metallic Bi_2Se_3 thin films, where top and bottom surfaces are connected though bulk electrons [21,22]. The change to $\alpha \approx 0$ observed for $t \leq 3$ QL is in accord with the diminishment of the surface transport channel and the eventual localization of the bulk state. A similar tendency was also observed in previous studies [23–25], although the decrease in α was less pronounced, probably due to a larger metallicity of the measured samples.

Now we discuss the origin of our observations. As was already found in Bi_2Se_3 ultrathin films by ARPES [19], an energy gap in the SS opens at the Dirac point below $t_c \simeq 6$ QL. Obviously, our transport measurements reflect this change in the Dirac dispersion. The gap is due to hybridization between top and bottom surfaces [schematically shown in the Fig. 4(b) inset], and such a hybridization gap Δ changes the massless Dirac dispersion $E = \pm\hbar v_F k$ into a massive one $E = \pm\sqrt{(\hbar v_F k)^2 + (\Delta/2)^2}$ [29,34]. For Bi_2Se_3, Δ is about 0.25 eV at $t = 2$ QL [19]. In our films, the Fermi level is estimated to be ~0.16 eV above the Dirac point, so even in our thinnest film the Fermi level is not in the gap but crosses the SS as schematically shown in the inset of Fig. 4(b). Hence, the observed drastic suppression of the surface transport is *not* due to the disappearance of surface carriers but is likely due to an enhanced scattering of the carriers [47].

The gap opening also has a profound effect on the Berry phase ϕ_B of the surface band $\psi_k(r)$. In the simplest case, ϕ_B is given by [34]

$$\phi_B = -i\int_0^{2\pi} d\varphi \left\langle \psi_k(r) \left| \frac{\partial \psi_k(r)}{\partial \varphi} \right\rangle = \pi\left(1 - \frac{\Delta}{E_F}\right), \quad (2)$$

and hence the Berry phase is reduced from π when a gap opens. This lifts the immunity of the SS from weak localization. Also, this change in ϕ_B weakens the WAL in the SS [35]. It is useful to note that in Fig. 4(a) the WAL was still observed for $t = 5$ QL which is below t_c, but this is natural because the small Δ at this t [19] makes the deviation of ϕ_B from π to be small.

More importantly, in the gapped phase, the SS becomes degenerate [29], which means that now for each momentum both up and down spin states are available. This opens the backscattering channel and significantly reduces the surface mobility. Actually, the hybridization of top and bottom surfaces means that the system is no longer truly three-dimensional (3D), so it is natural that the topological properties of 3D TIs are lost in the gapped phase, in full agreement with recent *ab initio* density functional studies of TI thin films [30,31]. In this respect, the present observation is a spectacular manifestation of the topological protection of the SS in 3D TIs.

We thank V. G. Mansurov for helpful suggestions about MBE growth. We also thank S. Oh, M. Sato, and Y. Tanaka for useful discussions. This work was supported by JSPS (NEXT Program), MEXT (Innovative Area "Topological Quantum Phenomena" KAKENHI), and AFOSR (AOARD 104103 and 124038).

*y_ando@sanken.osaka-u.ac.jp

[1] M. Z. Hasan and C. L. Kane, Rev. Mod. Phys. **82**, 3045 (2010).
[2] J. E. Moore, Nature (London) **464**, 194 (2010).
[3] X.-L. Qi and S.-C. Zhang, Rev. Mod. Phys. **83**, 1057 (2011).
[4] L. Fu and C. L. Kane, Phys. Rev. Lett. **100**, 096407 (2008).
[5] D. X. Qu, Y. S. Hor, J. Xiong, R. J. Cava, and N. P. Ong, Science **329**, 821 (2010).
[6] Z. Ren, A. A. Taskin, S. Sasaki, K. Segawa, and Y. Ando, Phys. Rev. B **82**, 241306(R) (2010).
[7] J. G. Analytis, R. D. McDonald, S. C. Riggs, J.-H. Chu, G. S. Boebinger, and I. R. Fisher, Nature Phys. **6**, 960 (2010).
[8] A. A. Taskin, Z. Ren, S. Sasaki, K. Segawa, and Y. Ando, Phys. Rev. Lett. **107**, 016801 (2011).
[9] B. Sacépé, J. B. Oostinga, J. Li, A. Ubaldini, N. J. G. Couto, E. Giannini, and A. F. Morpurgo, Nature Commun. **2**, 575 (2011).
[10] Z. Ren, A. A. Taskin, S. Sasaki, K. Segawa, and Y. Ando, Phys. Rev. B **84**, 075316 (2011).
[11] S. S. Hong, J. J. Cha, D. Kong, and Y. Cui, Nature Commun. **3**, 757 (2012).

[12] Z. Ren, A. A. Taskin, S. Sasaki, K. Segawa, and Y. Ando, Phys. Rev. B **85**, 155301 (2012).
[13] X. Chen, X.-C. Ma, K. He, J.-F. Jia, and Q.-K. Xue, Adv. Mater. **23**, 1162 (2011).
[14] G. Zhang, H. Qin, J. Teng, J. Guo, Q. Guo, X. Dai, Z. Fang, and K. Wu, Appl. Phys. Lett. **95**, 053114 (2009).
[15] A. Richardella, D. M. Zhang, J. S. Lee, A. Koser, D. W. Rench, A. L. Yeats, B. B. Buckley, D. D. Awschalom, and N. Samarth, Appl. Phys. Lett. **97**, 262104 (2010).
[16] H. D. Li, Z. Y. Wang, X. Kan, X. Guo, H. T. He, Z. Wang, J. N. Wang, T. L. Wong, N. Wang, and M. H. Xie, New J. Phys. **12**, 103038 (2010).
[17] N. Bansal *et al.*, Thin Solid Films **520**, 224 (2011).
[18] M. Lang, L. He, F. Xiu, X. Yu, J. Tang, Y. Wang, X. Kou, W. Jiang, A. V. Fedorov, and K. L. Wang, ACS Nano **6**, 295 (2012).
[19] Y. Zhang *et al.*, Nature Phys. **6**, 584 (2010).
[20] P. Cheng *et al.*, Phys. Rev. Lett. **105**, 076801 (2010).
[21] J. Chen, X. Y. He, K. H. Wu, Z. Q. Ji, L. Lu, J. R. Shi, J. H. Smet, and Y. Q. Li, Phys. Rev. B **83**, 241304(R) (2011).
[22] H. Steinberg, J. B. Laloë, V. Fatemi, J. S. Moodera, and P. Jarillo-Herrero, Phys. Rev. B **84**, 233101 (2011).
[23] Y. S. Kim, M. Brahlek, N. Bansal, E. Edrey, G. A. Kapilevich, K. Iida, M. Tanimura, Y. Horibe, S.-W. Cheong, and S. Oh, Phys. Rev. B **84**, 073109 (2011).
[24] M. Liu *et al.*, Phys. Rev. B **83**, 165440 (2011).
[25] N. Bansal, Y. S. Kim, M. Brahlek, E. Edrey, and S. Oh, arXiv:1104.5709.
[26] T. Ando, T. Nakanishi, and R. Saito, J. Phys. Soc. Jpn. **67**, 2857 (1998).
[27] J. Linder, T. Yokoyama, and A. Sudbo, Phys. Rev. B **80**, 205401 (2009).
[28] C.-X. Liu, H. J. Zhang, B. Yan, X.-L. Qi, T. Frauenheim, X. Dai, Z. Fang, and S.-C. Zhang, Phys. Rev. B **81**, 041307(R) (2010).
[29] H.-Z. Lu, W.-Y. Shan, W. Yao, Q. Niu, and S.-Q. Shen, Phys. Rev. B **81**, 115407 (2010).
[30] K. Park, J. J. Heremans, V. W. Scarola, and D. Minic, Phys. Rev. Lett. **105**, 186801 (2010).
[31] J. Chang, L. F. Register, S. K. Banerjee, and B. Sahu, Phys. Rev. B **83**, 235108 (2011).
[32] T. Sato, K. Segawa, K. Kosaka, S. Souma, K. Nakayama, K. Eto, T. Minami, Y. Ando, and T. Takahashi, Nature Phys. **7**, 840 (2011).
[33] X.-L. Qi, T. L. Hughes, and S.-C. Zhang, Phys. Rev. B **78**, 195424 (2008).
[34] H.-Z. Lu, J. Shi, and S.-Q. Shen, Phys. Rev. Lett. **107**, 076801 (2011).
[35] H.-Z. Lu and S.-Q. Shen, Phys. Rev. B **84**, 125138 (2011).
[36] Two-step deposition growth has been applied to various systems in the past. For Bi_2Se_3, it has been recently reported in Refs. [16,17].
[37] See Supplemental Material at http://link.aps.org/supplemental/10.1103/PhysRevLett.109.066803 for supplemental data and discussions.
[38] M. Bianchi, D. Guan, S. Bao, J. Mi, B. B. Iversen, P. D. C. King, and P. Hofmann, Nature Commun. **1**, 128 (2010).
[39] D. Shoenberg, *Magnetic Oscillations in Metals* (Cambridge University Press, Cambridge, England, 1984).
[40] Y. Xia *et al.*, Nature Phys. **5**, 398 (2009).
[41] T. Hanaguri, K. Igarashi, M. Kawamura, H. Takagi, and T. Sasagawa, Phys. Rev. B **82**, 081305(R) (2010).
[42] Similar upward band bending has been observed in pure Bi_2Se_3 crystals [J. G. Analytis, J.-H. Chu, Y. Chen, F. Corredor, R. D. McDonald, Z. X. Shen, and I. R. Fisher, Phys. Rev. B **81**, 205407 (2010)], in Sb-doped Bi_2Se_3 crystals [7], and in $Bi_{1.5}Sb_{0.5}Te_{1.7}Se_{1.3}$ crystals [8], so it is not unusual.
[43] J. Xiong, Y. Luo, Y.-H. Khoo, S. Jia, R. J. Cava, and N. P. Ong, arXiv:1111.6031.
[44] A. A. Taskin and Y. Ando, Phys. Rev. B **84**, 035301 (2011).
[45] N. W. Ashcroft and D. N. Mermin, *Solid State Physics* (Holt-Saunders, Tokyo, 1976).
[46] S. Hikami, A. I. Larkin, and Y. Nagaoka, Prog. Theor. Phys. **63**, 707 (1980).
[47] In a very recent paper reporting SdH oscillations in a 6-QL film [L. He *et al.*, Nano Lett. **12**, 1486 (2012)], the Fermi level was pinned in the gap and hence the detected physics was different. Similarly, an insulating behavior has been observed in an exfoliated 3.5-nm-thick crystal, but it was realized by tuning the Fermi level into the gap by gating [S. Cho, N. P. Butch, J. Paglione, and M. S. Fuhrer, Nano Lett. **11**, 1925 (2011)].